J Mater Sci (2010) 45:865–870
DOI 10.1007/s10853-009-4012-8

High-temperature oxidation of $MoSi_2$

A. A. Sharif

Received: 26 June 2009 / Accepted: 30 October 2009 / Published online: 10 November 2009
© Springer Science+Business Media, LLC 2009

Abstract Oxidation behavior of $MoSi_2$ was investigated in air over the temperature range of 1400–1700 °C. Spallation of the SiO_2 scale did not occur at any temperature, and Mo_5Si_3 formation did not happen below 1700 °C. A change in the rate-controlling mechanism was detected within the temperature range of this study. Activation energy for oxidation of $MoSi_2$ at high temperatures was determined to be 204 kJ/mol. This value is less than the value of activation energy for oxidation of $MoSi_2$ controlled by diffusion of O_2 through amorphous SiO_2 layer reported at lower temperatures. The decrease in activation energy is attributed to the increased degree of crystallization of amorphous silica to β-cristobalite at high temperatures resulting in enhanced O_2 diffusion through SiO_4^{-4} tetrahedral structure.

Introduction

Because of their outstanding high-temperature stability, molybdenum disilicide ($MoSi_2$) alloys are being investigated for applications as high-temperature structural materials [1, 2]. These alloys could replace superalloys to increase the operating temperature and, consequently, the efficiency of gas engines. Even a minor increase in the efficiency of an engine results in significant savings in fuel costs and reduction in harmful emissions. However, $MoSi_2$-based alloys have low fracture toughness and are prone to pest oxidation at low temperatures. At high temperatures, they have low strengths, and their oxide scale may be prone to spallation. Nonetheless, it has been shown that the pest oxidation problem may be overcome by alloying and processing techniques [3, 4], and both low-temperature ductility and high-temperature strength may be improved by alloying [5, 6]. Spallation of oxide scale in $MoSi_2$ is a serious problem, but this drawback has not been reported by all investigators [7, 8]. Spallation of oxide scale in $MoSi_2$ arises from three sources: thermal shock experienced during heating or cooling, volume change due to phase transformations, or build up of gaseous reaction products under the oxide scale.

$MoSi_2$ has outstanding oxidation resistance up to 1700 °C, which results from the formation of a protective silica (SiO_2) layer above the pesting temperature [9]. This is typical of all SiO_2-forming materials. Above the pest oxidation temperature range, ~500–800 °C, oxidation behavior of $MoSi_2$ is identical to that of Si up to 1400 °C [10]. During oxidation at higher temperatures, a continuous SiO_2 layer forms on $MoSi_2$, which acts as a barrier against further oxidation [11]. The formation and growth of the oxide layer on $MoSi_2$ is governed by transport of the oxidizing species to the outer surface of the oxide layer for absorption, diffusion of the oxidant through the oxide layer, and oxidant reaction with the bulk $MoSi_2$ to form SiO_2. Simultaneous solution of the differential equations of these processes results in two equations, one for short times, $x = k_l(t + \tau)$, and another for long times, $x^2 = k_p t$, as described in detail by Deal and Grove [12]. Here x is the oxide thickness at time t, τ is the time required to form the initial thickness of the oxide layer, and k_l and k_p are the linear and parabolic oxidation rate constants, respectively. The linear rate is a consequence of interfacial reaction control at short times, and diffusion of the reactants is the controlling mechanism at longer times in the parabolic

A. A. Sharif (✉)
Department of Mechanical Engineering, California State University, Los Angeles, 5151 State University Dr., Los Angeles, CA 90032-8153, USA
e-mail: aasharif@calstatela.edu

regime. The kinetics of high-temperature oxidation of $MoSi_2$ may be studied by measuring either the increase in the thickness of the oxide layer or the weight gain from absorption of oxygen into the sample versus time at any given temperature. The linear and parabolic rate constants may be calculated by either method. These rate constants may be used to estimate the time to form a certain oxide thickness or the life expectancy of a part made from $MoSi_2$ or its alloys at a given temperature in an oxidizing environment.

Although many studies have been conducted on the kinetics of oxidation of $MoSi_2$, there are only limited investigations at temperatures approaching the melting temperature of the oxide scale [13–17], which is the higher temperature limit for application of $MoSi_2$-based alloys [18, 19]. The complex oxidation kinetics of $MoSi_2$ results from (a) pesting, (b) formation of molybdenum oxides, (c) formation of different molybdenum silicides, i.e., Mo_5Si_3 and Mo_3Si, during oxidation, (d) transformation of the SiO_2 scale into its various phases, and (e) cracking and spallation of the oxide layer. Depending on experimental conditions, one or more of these occurrences may affect the kinetics of oxidation. Pesting and formation of molybdenum oxides are, however, low-temperature phenomena and are not concerns at high temperatures. The presence of Mo_5Si_3 has been reported at both low- and high-temperatures [13, 20–22], whereas Mo_3Si has been observed to result from the reaction of Mo_5Si_3 with O_2 at low temperatures [23]. Mo_5Si_3 forms beneath the oxide scale. Thus, upon formation of a stable oxide layer, Mo_5Si_3 is insulated from oxygen. At high temperatures rapid oxide scale formation prevents formation of Mo_3Si.

Under ultra-high temperatures, it is unclear whether a change in the kinetics of oxidation of $MoSi_2$ results from phase transformation, instability of the oxide layer, or Mo_5Si_3 formation under the oxide scale. Moreover, the presence of a change in the oxidation mechanism at temperatures over 1400 °C has not yet been identified. Maruyama et al. [14–17] have already investigated oxidation behavior of $MoSi_2$ at high temperatures; however, extensive oxide scale spallation at 1550 °C and liquidity of the oxide scale at 1775 °C would hinder confirming the presence or absence of a change in the oxidation mechanism. Since scale growth is a diffusion-controlled process, the extent of crystallization, crystal structure of SiO_2, and formation of Mo_5Si_3 diffusion barrier layer may all affect diffusion and, consequently, oxidation mechanism. Therefore, this investigation aims to validate the presence of a change in oxidation mechanism above 1400 °C by focusing on the ultra-high-temperature kinetics of oxidation of $MoSi_2$ when oxide scale crystallization takes place when compared to oxidation regimes where only an amorphous SiO_2 layer forms.

Experimental procedure

Polycrystalline unalloyed $MoSi_2$ buttons were prepared by arc-melting elemental Mo with 99.95% purity and Si with 99.999% purity in an argon atmosphere. Following the results of previous investigations, excess Si was used to compensate for the Si loss that occurs during arc-melting [24]. The starting composition of the alloy was $MoSi_{2.01}$. During arc-melting, each sample was turned over and re-melted four times to ensure homogeneity. Figure 1 is the XRD of a sample that was crushed after arc-melting. It indicates that no secondary phases existed in the as-prepared samples.

The presence of cracks on the sample surface would result in enhanced oxidation rates. In order to eliminate introduction of microcracks on the sample surface during polishing, a decision was made not to polish the as-melted samples before oxidation experiments. These samples were buttons with a base diameter of about 11 mm and height of about 6 mm. The surface area of the samples was estimated by calculating areas of the strips that would be obtained by cutting disks parallel to the base of the droplet and opening these disks to obtain trapezoidal surfaces.

These samples were ultrasonically cleaned in methanol, dried, and weighed using a microbalance with accuracy of 0.1 μg. The samples were placed in an air-furnace at designated temperatures and were allowed to oxidize for 3, 13, 25, 50, 75, and 100 h. Furnace heating and cooling rate was about 25°/min. After each oxidation interval, the samples were allowed to cool down in the furnace prior to weighing. Upon completion of 100 h of oxidation, samples were sectioned and polished on one side to remove the oxide layer and to expose the cross section of the oxide layer on the other sides. Oxide thickness measurements were performed on micrographs of the cross section of the oxide scale obtained by scanning electron microscopy (SEM).

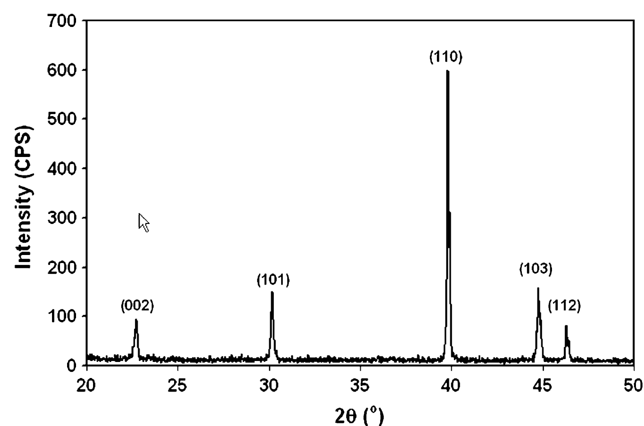

Fig. 1 The room temperature XRD pattern of $MoSi_2$ powder obtained from crushed buttons that were prepared with starting composition of $MoSi_{2.01}$

Composition of the phases present was determined by energy-dispersive X-ray spectrometer (EDS).

Results and discussion

The plots of specific weight gain versus time for isothermal oxidation of $MoSi_2$ at 1400, 1550, and 1700 °C are shown in Fig. 2. Oxidation of $MoSi_2$ at all the three temperatures started with a rapid weight gain followed by a slower rate of oxidation. During the initial part of oxidation, when a protective layer of oxide had not yet formed, oxygen was readily available to react with silicon, and a rapid oxidation rate was observed. This is the region whose slope is the linear rate constant for the oxygen–silicon reaction, which is available in the literature [21] and will not be calculated here. Here it is assumed that linear oxidation is complete within the first 3 h, which is an accurate estimation since it has been shown that the linear oxidation ends rapidly at the temperatures tested in this study [13].

As oxide nuclei grow during the linear oxidation regime, they flow sideways to cover the sample insulating it from the surrounding oxygen [13]. From this point onward, Si and O_2 must diffuse through the bulk material and the oxide layer, respectively, to arrive at the SiO_2–$MoSi_2$ interface for oxidation reaction to take place. The linear oxidation regime ends and a parabolic regime starts when an oxide layer covers the sample. As oxidation time increases, the oxidation rate decreases. The plot of specific weight gain versus time should be parabolic if oxidation is diffusion-controlled. The dashed lines, which represent polynomial of second order, closely follow the experimental data at all the three temperatures. The parabolic oxidation rate, k_p, may be calculated from the slope of the line obtained by plotting weight gain square (ΔW^2) versus

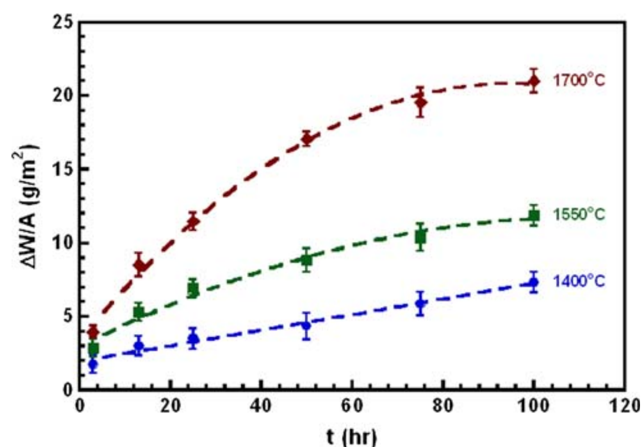

Fig. 2 Plots of specific weight gain at three test temperatures during isothermal oxidation of $MoSi_2$

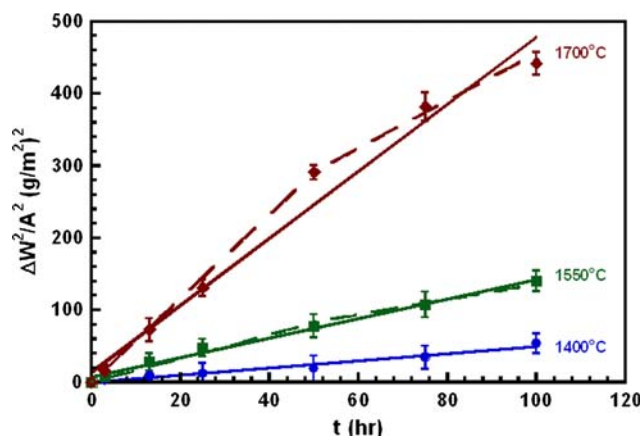

Fig. 3 Plots of specific weight gain square (ΔW^2) versus time (t) at the three test temperatures during oxidation of $MoSi_2$

time (t), as shown in Fig. 3. Clearly, there is a change in the rate of oxidation with increasing temperature and time. In addition to a change in oxidation rate, which occurs as a result of the transition from linear to parabolic oxidation (not shown in the figure), there seems to be another change of slope around 50 h. This is shown for the samples oxidized at 1550 and 1700 °C by dashed lines in Fig. 3. The change in the rate constants becomes more pronounced with increasing temperature. Such a change in the parabolic rate constant has been reported, and it is generally believed to be a result of transformation from one silica phase to another [25].

The parabolic rate constants calculated from the slopes of the lines in Fig. 3 are 0.33, 0.92, and 3.2 $g^2/(m^4\ h)$ at 1400, 1550, and 1700 °C, respectively. SEM micrographs of the cross sections of the samples after 100 h of oxidation at 1400 °C (a), 1550 °C (b), and 1700 °C (c) are shown in Fig. 4. The average oxide thicknesses for these samples are 1.4 ± 0.08 μm (a), 2.5 ± 0.2 μm (b), and 17.8 ± 1.3 μm (c). Compared to the oxidation behavior of $MoSi_2$ at lower temperatures, there are major differences at 1700 °C. Specifically, the oxide layers on the samples oxidized at the two lower temperatures were relatively uniform in thickness, and no spallation or cracks could be found in the scale. However, the sample oxidized at 1700 °C shows relatively large variations in oxide thickness as well as cracks in the oxide scale throughout the sample. Also, a third phase was observed under the SiO_2 scale of this sample that was continuous at some regions and remained isolated at other regions.

This third phase between the $MoSi_2$ and SiO_2 layers, which can be observed as lighter than the other two phases in the back-scattered electron (BSE) micrograph in Fig. 4c, is a Mo-rich phase. Quantitative analysis indicated that the third phase was Mo_5Si_3, which had formed as Si was consumed rapidly through oxidation to form the oxide

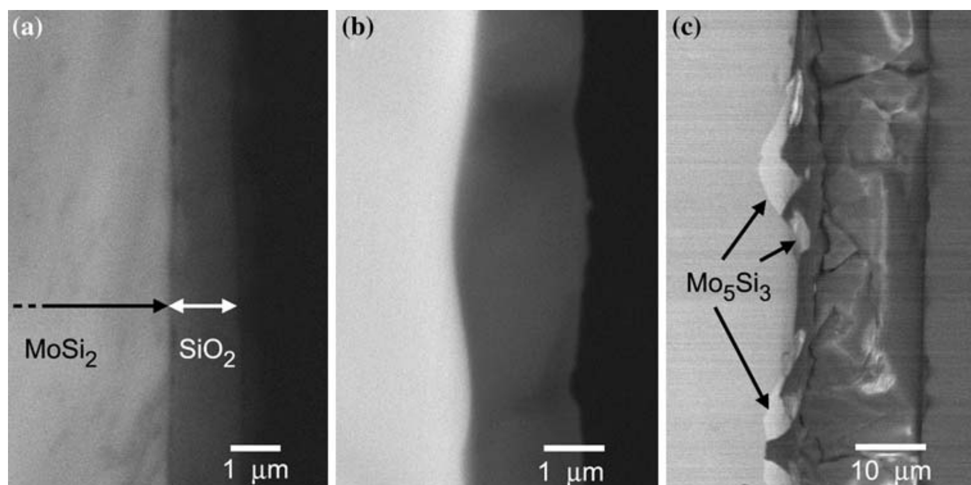

Fig. 4 BSE micrographs of cross sections of $MoSi_2$ samples oxidized in air at 1400 °C (**a**), 1550 °C (**b**), and 1700 °C (**c**)

layer. The two possible reactions for oxidation of $MoSi_2$ are as follows:

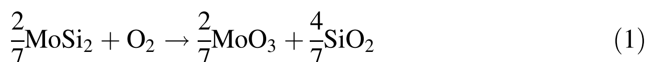

$$\frac{2}{7}MoSi_2 + O_2 \rightarrow \frac{2}{7}MoO_3 + \frac{4}{7}SiO_2 \quad (1)$$

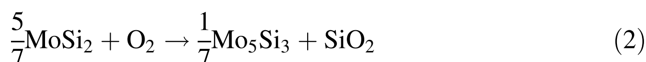

$$\frac{5}{7}MoSi_2 + O_2 \rightarrow \frac{1}{7}Mo_5Si_3 + SiO_2 \quad (2)$$

Calculations based on 1 mol of O_2 indicate that the absolute value of the Gibbs free energy change for reaction (2) is greater than the one for reaction (1) [26]. Therefore, reaction (2) is thermodynamically favored over reaction (1) until all the Si is consumed and Mo_5Si_3 further oxidized to form Mo_3Si. Mo_3Si in the presence of oxygen would further oxidize to produce SiO_2 and MoO_3 [27]. No sign of bubbling of the oxide scale was detected; therefore, MoO_3 did not form beneath the scale under the conditions of these experiments.

Mo_5Si_3 formation was not observed in the samples oxidized at 1400 and 1550 °C. However, at 1700 °C the oxide scale crystallizes into cristobalite, which results in enhanced diffusion of oxygen through the oxide scale. This results in rapid consumption of Si beneath the oxide scale through oxidation, leaving excess Mo, which explains the formation of Mo_5Si_3 at higher temperatures. Maruyama et al. [14] observed a layer of Mo_5Si_3 even at 1550 °C. They started with a 1/2 Mo/Si molar ratio for samples prepared by arc-melting. During arc-melting, vaporization of Si resulted in an alloy that was Si-deficient. In a later publication [15], it was reported that their Mo/Si molar ratio was actually 33.9:66.1 in the samples that were prepared with 1/2 molar ratio. Such an alloy is prone to Mo_5Si_3 formation during oxidation without the need for local Si depletion by oxidation. Maruyama et al. [14] also observed spallation of the oxide scale at 1550 °C, contrary to our findings. Spallation observed in their work may have resulted from increased stress experienced by their samples caused be volumetric mismatch during thermal shock under rapid cooling rate of 3 °C/s in addition to volumetric mismatch caused by phase transformation.

Mo_5Si_3 was most heavily concentrated where there was a spike in the thickness of the oxide layer. This occurred because the oxidation rate was greatest at those points. At 1700 °C, the stable phase of SiO_2 is β-cristobalite. As the sample cools down to room temperature β-cristobalite is unstable below $\sim$270 °C where there is β–α transformation of cristobalite, which is associated with 5% volume change [28]. Residual stresses due to volumetric mismatch result in the generation of cracks as seen in Fig. 4c. Spikes seen in the oxide scale do not coincide with these cracks because oxidant access through cracks only happened during the early stages of the intervals of oxidation at 1700 °C when the sample was returned into the furnace after it was removed for weight measurement. As the sample temperature was raised to 1700 °C, the oxide layer was healed, preventing further easy access for the oxidant. The next sample retrieval resulted in a new set of cracks which would introduce a new set of spikes in the oxide thickness during oxidation.

Since oxidation is a thermally activated process, oxide growth rate may be described by an Arrhenius type relationship:

$$k_p = k_o \exp\left(-\frac{Q}{RT}\right)$$

where Q is the activation energy for oxidation, R is the gas constant, T is the absolute temperature, and k_o is a constant. Activation energy of 204 kJ/mol for oxidation of $MoSi_2$ from 1400 to 1700 °C was calculated from the slope of logarithm of parabolic rate constant, ln (k_p), versus inverse absolute temperature, $1/T$, as shown in Fig. 5. Reported

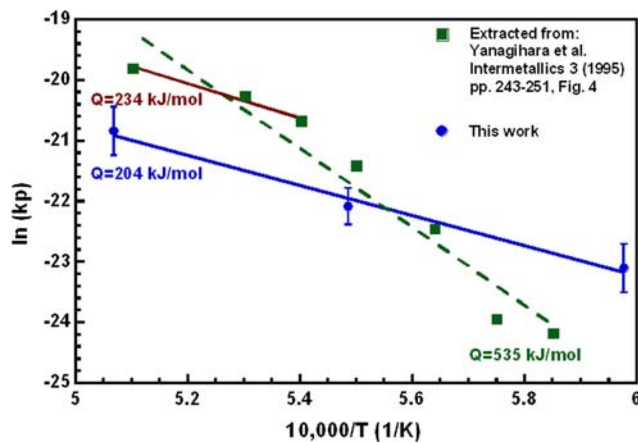

Fig. 5 Plot of logarithm of parabolic rate constant ln (k_p) versus inverse absolute temperature (1/*T*) for determining activation energy for oxidation of $MoSi_2$ from 1400 to 1700 °C. Data points for the Yanagihara et al. work were extracted from Figure 4 of Ref. [16]

values of activation energy for the oxidation of $MoSi_2$ are 340 kJ/mol at 1164–1500 °C [20], 343 kJ/mol at 900–1200 °C [29], and 298 kJ/mol at 925–1225 °C [30]. The similarity of these values indicates that there is no change in the oxidation mechanism of $MoSi_2$ from pest oxidation temperature to ~1500 °C. Yanagihara et al. [16] reported activation energy of 535 kJ/mol in the temperature range of ~1450 to ~1700 °C. The values of their data points were extracted from a figure in [16] and are plotted in Fig. 5 for comparison. The value of 538 kJ/mol was calculated from their data over the entire temperature range, thus confirming the relative accuracy of the estimations. The linear regression line fit to their data is shown in Fig. 5 as a dashed line. As evident in the figure, their two highest temperature data points deviate from the linear behavior of the rest of their data. Calculating the value of *Q* for their three and two highest temperature data points, the values of 234 and 191 kJ/mol, respectively, were estimated for activation energy. The linear regression fit to their last three data points is also shown in the figure as a solid line. Clearly, there is a change in the mechanism of oxidation at higher temperatures indicated by the similarity of the slopes of the lines fit into the data of this work with those of the three highest temperature data points of Ref. [16]. The value of *Q* is lower than those reported at lower temperatures where diffusion of O_2 through amorphous SiO_2 is the rate controlling mechanism.

Since a cohesive layer of Mo_5Si_3 was observed beneath some segments of the oxide layer, the possibility of a rate controlling mechanism by diffusion of Si through the Mo_5Si_3 layer was considered. However, that would require an increase in the activation energy when compared to lower temperatures caused by the presence of a new diffusion barrier, which contradicts the result obtained here. The increased degree of crystallization at higher temperatures and longer times enhances O_2 diffusion through the oxide layer. As the degree of crystallization of SiO_2 into β-cristobalite is increased at higher temperatures, enhanced ordering of SiO_4^{-4} tetrahedra in β-cristobalite allows for easier diffusion of O_2 molecules resulting in lower activation energy than the values reported at lower temperatures. More investigation at intermediate temperatures is needed to determine the temperature at which the change occurs.

Conclusions

Oxide scale spallation at high temperatures is not an inherent property of $MoSi_2$ and may result from experimental conditions. At temperatures approaching the melting temperature of SiO_2, there is a change in oxidation mechanism of $MoSi_2$ when compared to lower temperatures. The activation energy for oxidation decreased from ~340 kJ/mol at lower temperatures to 204 kJ/mol above 1550 °C.

Acknowledgements SEM investigations were made possible through the use of ESEM procured by National Science Foundation MRI Grant number CMS-0321226. This research was, in part, supported by the National Science Foundation CREST Grant HRD-0932421.

References

1. Vasudevan AK, Petrovic JJ (1992) Mater Sci Eng A 155:1
2. Petrovic JJ (1997) Ceram Eng Sci Proc 18:3
3. Hebsur MG, Nathal MV (1997) Structural intermetallics. The Minerals, Metals and Materials Society, Warrendale
4. Kurokawa K, Houzumi H, Saeki I, Takahashi H (1999) Mater Sci Eng A 261:292
5. Sharif AA, Misra A, Mitchell TE (2005) Scripta Mater 52:399
6. Inui H, Ishikawa K, Yamaguchi M (2000) Intermetallics 8:1131
7. Schneibel JH, Sekhar JA (2003) Mater Sci Eng A 340:204
8. Nyutu EK, Kmetz MA, Suib SL (2006) Surf Coat Technol 200:3980
9. Schlichting J (1979) Mater Chem 4:93
10. Grabke HJ, Meier GH (1995) Oxid Met 44:147
11. Mitra R, Rao VVR, Mahajan YR (1997) Mater Sci Technol 13:415
12. Deal BE, Grove AS (1965) J Appl Phys 36:3770
13. Berkowitz-Mattuk JB, Dils RR (1965) J Electrochem Soc 112:583
14. Maruyama T, Yanagihara K, Nagata K (1993) Corros Sci 35:939
15. Yanagihara K, Maruyama T, Nagata K (1993) Mater T JIM 34:1200
16. Yanagihara K, Maruyama T, Nagata K (1995) Intermetallics 3:243
17. Maruyama T, Yanagihara K (1997) Mater Sci Eng A 239–240:828
18. Searcy AW (1957) J Am Ceram Soc 40:431
19. Jeng YL, Lavernia EJ (1994) J Mater Sci 29:2557. doi: 10.1007/BF00356804
20. Wirkus CD, Wilder DR (1966) J Am Ceram Soc 49:173

21. Zhu YT, Stan M, Conzone SD, Butt DP (1999) J Am Ceram Soc 82:2785
22. Ito K, Hayashi T, Yokobayashi M, Numakura H (2004) Intermetallics 12:407
23. Natesan K, Deevi SC (2000) Intermetallics 8:1147
24. Sharif AA, Misra A, Petrovic JJ, Mitchell TE (2001) Intermetallics 9:869
25. Narushima T, Goto T, Hirai T (1989) J Am Ceram Soc 71:1386
26. Liu YQ, Shao G, Tsakiropoulos P (2001) Intermetallics 9:125
27. Shaw L, Abbaschian R (1995) J Mater Sci 30:5272. doi:10.1007/BF01178416
28. Gai-Boyes PL, Saltzberg MA, Vega A (1993) J Solid State Chem 106:35
29. Glushko PI, Dorokohov VI, Ncchiporenko YP (1963) Phys Metals Metallogr 13:111
30. Sucov EW (1963) J Am Ceram Soc 46:14